

# Lateral diffusion induced by active proteins in a biomembrane

Yuto Hosaka, Kento Yasuda, Ryuichi Okamoto, and Shigeyuki Komura\*

*Department of Chemistry, Graduate School of Science and Engineering,*

*Tokyo Metropolitan University, Tokyo 192-0397, Japan*

(Dated: March 14, 2017)

We discuss the hydrodynamic collective effects due to active protein molecules that are immersed in lipid bilayer membranes and modeled as stochastic force dipoles. We specifically take into account the presence of the bulk solvent which surrounds the two-dimensional fluid membrane. Two membrane geometries are considered: the free membrane case and the confined membrane case. Using the generalized membrane mobility tensors, we estimate the active diffusion coefficient and the drift velocity as a function of the size of a diffusing object. The hydrodynamic screening lengths distinguish the two asymptotic regimes of these quantities. Furthermore, the competition between the thermal and non-thermal contributions in the total diffusion coefficient is characterized by two length scales corresponding to the two membrane geometries. These characteristic lengths describe the crossover between different asymptotic behaviors when they are larger than the hydrodynamic screening lengths.

## I. INTRODUCTION

Biomembranes consisting of lipid bilayers can be regarded as thin two-dimensional (2D) fluids, and membrane protein molecules as well as lipid molecules are allowed to move laterally [1, 2]. These membrane inclusions are subject to the thermal motion of lipid molecules, leading to random positional fluctuations. Such a Brownian motion plays important roles in various life processes such as transportation of materials or reaction between chemical species [3]. In order to describe lateral diffusion of membrane proteins, a drag coefficient of a cylindrical disc moving in a 2D fluid sheet has been theoretically studied in various membrane environments [4–10]. The obtained drag coefficient was used to estimate the diffusion coefficients of membrane proteins through Einstein’s relation under the assumption that the system is in thermal equilibrium [11].

In recent experiments, however, it has been shown that motions of particles inside cells are dominantly driven by random non-thermal forces rather than thermal fluctuations [12, 13]. In these experimental works, they found that non-thermal forces in biological cells are generated by active proteins undergoing conformational changes with a supply of adenosine triphosphate (ATP). These active fluctuations lead to enhanced diffusion of molecules in the cytoplasm [14, 15]. Biomembranes also contain various active proteins which, for example, act as ion pumps by changing their shapes to exert forces to the adjacent membrane and solvent [2]. Lipid bilayers containing such active proteins have been called “active membranes”, and their out-of-plane fluctuations (deformations) have already been investigated both experimentally and theoretically [16–18]. However, lateral motions of inclusions in membranes that are induced by active proteins have not yet been considered. Since such active forces give rise to enhanced diffusion, one needs to

take into account both active non-thermal fluctuations as well as passive thermal ones to calculate diffusion in membranes.

Recently, Mikhailov and Kapral discussed an enhanced diffusion due to non-thermal fluctuating hydrodynamic flows which are induced by oscillating active force dipoles [see Fig. 1(a)] [19, 20]. They calculated the active diffusion coefficient of a passive particle immersed either in a three-dimensional (3D) cytoplasm or in a 2D membrane, and showed that it exhibits a logarithmic size dependence for the 2D case. Moreover, a chemotaxis-like drift of a passive particle was predicted when gradients of active proteins or ATP are present [19]. Later Koyano *et al.* showed that lipid membrane rafts, in which active proteins are concentrated, can induce a directed drift velocity near the interface of a domain [21]. In these works, they considered membranes that are smaller in size than the hydrodynamic screening length. Huang *et al.* performed coarse-grained simulations of active protein inclusions in lipid bilayers [22, 23]. In Ref. [23], they showed that active proteins undergoing conformational motions not only affect the membrane shape but also laterally stir the lipid bilayer so that lipid flows are induced. Importantly, the flow pattern induced by an immobilized protein resembles the 2D fluid velocity fields that are created by a force dipole.

Following Refs. [19, 20], we assume that an active protein behaves as an oscillating force dipole which acts on the surroundings to generate hydrodynamic flows that can induce motions of passive particles in the fluid. In this paper, we investigate active diffusion and drift velocity of a particle in “free” and “confined” membranes which are completely flat and infinitely large. In the free membrane case, a thin 2D fluid sheet is embedded in a 3D solvent having typically a lower viscosity than that of the membrane. Whereas in the confined case, which mimics a supported membrane [24], a membrane is sandwiched by two rigid walls separated by a finite but small distance from it. For both the free and confined membrane cases, we employ general mobility tensors that take into

---

\* komura@tmu.ac.jp

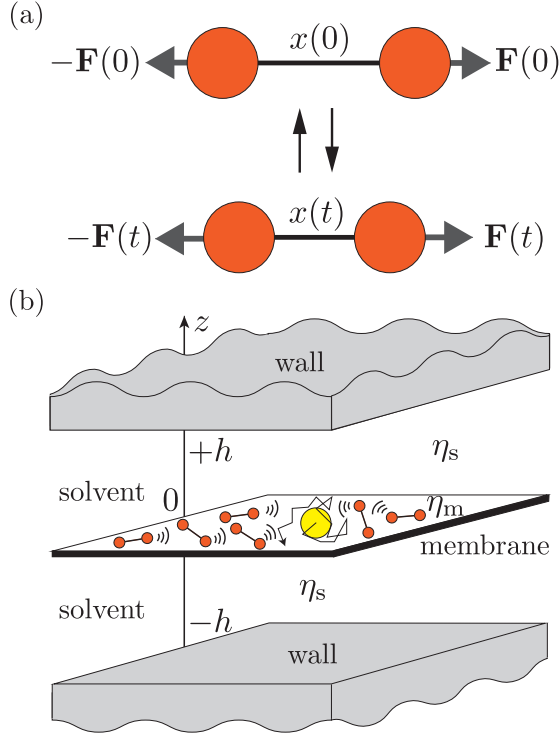


FIG. 1. (a) The conformational change of an oscillating force dipole representing an active protein. Within a turnover cycle of the force dipole separated by a distance  $x(t)$ , it exerts two oppositely directed forces  $\pm \mathbf{F}(t)$  at time  $t$ . The integral intensity of a force dipole is  $S$  (see the text). (b) Schematic picture showing a flat and infinitely large membrane of 2D viscosity  $\eta_m$  that is located at  $z = 0$ . The membrane is surrounded by a bulk solvent of 3D viscosity  $\eta_s$ , and the two flat walls are located at  $z = \pm h$ . The solvent velocity is assumed to vanish at the surfaces of these walls. The “free membrane” and the “confined membrane” cases correspond to the limits of  $h \rightarrow \infty$  and  $h \rightarrow 0$ , respectively. The yellow passive particle undergoes a Brownian motion due to thermal and non-thermal fluctuations. The latter contribution is induced by active force dipoles which are homogeneously distributed in the membrane with a 2D concentration  $c_0$ .

account the hydrodynamic effects mediated by the surrounding 3D solvent [25–27]. Using the general mobility tensors, we numerically calculate the active diffusion coefficient and the drift velocity as a function of the diffusing particle size for the entire length scales. Furthermore, several asymptotic expressions are also derived in order to compare with numerical estimates and thermal contributions. Importantly, our result leads to characteristic length scales describing a crossover from non-thermal to thermal diffusive behaviors for large scales.

In the next section, we present the expressions for the active diffusion coefficient and the drift velocity in 2D membranes [19]. We also review the general mobility tensors for the free and confined membrane cases [25–27]. Using these expressions, we calculate in Sec. III the active diffusion coefficient for the two geometries. In Sec. IV, we compare the thermal diffusion coefficient with the ob-

tained non-thermal diffusion coefficient, and discuss the characteristic crossover lengths. In Sec. V, we obtain the drift velocities as a function of the particle size. The summary of our work and some numerical estimates for the obtained quantities are given in Sec. VI.

## II. ACTIVE TRANSPORT AND MOBILITY TENSORS IN MEMBRANES

### A. Active diffusion coefficient

Active proteins in a 2D biological membrane, modeled as oscillating force dipoles, produce non-equilibrium fluctuations and cause an enhancement of the lateral diffusion of a passive particle. We assume that the spatially fixed force dipoles are homogeneously and isotropically distributed in the membrane, and they exert only in-plane lateral forces. The total diffusion coefficient is given by  $D = D_T + D_A$ , where  $D_T$  is the thermal contribution and determined by Einstein’s relation (which will be discussed in Sec. IV), and  $D_A$  is the active non-thermal contribution given by [19]

$$D_A = \frac{Sc_0}{2} \int d^2r \Omega_{\beta\beta'\gamma\gamma'} \frac{\partial G_{\alpha\beta}(\mathbf{r})}{\partial r_\gamma} \frac{\partial G_{\alpha\beta'}(\mathbf{r})}{\partial r_{\gamma'}}, \quad (1)$$

where  $\mathbf{r} = (x, y)$  denotes a 2D vector and we have introduced a notation

$$\Omega_{\beta\beta'\gamma\gamma'} = \frac{1}{8} (\delta_{\beta\beta'} \delta_{\gamma\gamma'} + \delta_{\beta\gamma} \delta_{\beta'\gamma'} + \delta_{\beta\gamma'} \delta_{\beta'\gamma}). \quad (2)$$

Throughout this paper, the summation over repeated greek indices is assumed. In Eq. (1),  $S$  is the integral intensity of a force dipole,  $c_0$  is the constant 2D concentration of active proteins, and  $G_{\alpha\beta}(\mathbf{r})$  is the membrane mobility tensor which will be discussed later separately.

Within a fluctuating “dimer model” as presented in Fig. 1(a), the magnitude of a force dipole is given by  $m(t) = x(t)F(t)$ , where  $x(t)$  is the distance between the two spheres and  $F(t)$  is the magnitude of the oppositely directed forces. Then the integral intensity  $S$  of a force dipole is given by  $S = \int_0^\infty dt \langle m(t)m(0) \rangle$ , where the bracket denotes the statistical average [19]. Since we assume that active proteins are homogeneously distributed in the membrane as shown in Fig. 1(b), it is sufficient to consider only the isotropic diffusion as given by Eq. (1).

In deriving Eq. (1), the size of a dipole is assumed to be much smaller than the distance between the passive particle and active force dipoles [19]. It should be noted, however, that the above expression is not accurate when the distance between them becomes smaller.

### B. Drift velocity

Although we have assumed above that  $c_0$  is constant, active proteins are often distributed inhomogeneously in

the membrane due to heterogeneous structures such as sphingolipid-enriched domains [28, 29]. According to the “lipid raft” hypothesis, these domains act as platforms for membrane signaling and trafficking [30]. Hence it is also important to consider the effects of nonuniform spatial distribution of active proteins and to see how it affects the lateral dynamics in membranes.

When a spatial concentration gradient  $\nabla c$  of active protein is present, it gives rise to an unbalanced induced forces between two points in the membrane. Hence passive particles are subjected to a drift toward either lower or higher concentration of active proteins, and a chemotaxis-like drift can occur. When the absolute value of the concentration gradient  $|\nabla c|$  is assumed to be constant, the induced drift velocity of a passive particle in the direction  $\nabla c$  is given by [19]

$$V = -S|\nabla c| \int d^2r \Omega_{\beta\beta'\gamma\gamma'} \hat{n}_\alpha \frac{\partial^2 G_{\alpha\beta}(\mathbf{r})}{\partial r_\gamma \partial r_\delta} \frac{\partial G_{\delta\beta'}(\mathbf{r})}{\partial r_{\gamma'}} (\mathbf{r} \cdot \hat{\mathbf{n}}). \quad (3)$$

Here, the unit vector  $\hat{\mathbf{n}} = \nabla c/|\nabla c|$  denotes the direction of the concentration gradient of active proteins. We shall employ the above expression to obtain the lateral drift velocity in a membrane by using the membrane mobility tensor as discussed below.

### C. Membrane mobility tensors

Since we discuss active diffusion in an infinitely large flat membrane, we use the 2D membrane mobility tensor which also takes into account the hydrodynamic effects of the surrounding 3D solvent. We consider a general situation as depicted in Fig. 1(b), where a fluid membrane of 2D shear viscosity  $\eta_m$  is surrounded by a solvent of 3D shear viscosity  $\eta_s$ . Furthermore, we consider the case in which there are two walls located symmetrically at an arbitrary distance  $h$  from the flat membrane [25–27].

We denote the in-plane velocity vector of the fluid membrane by  $\mathbf{v}(\mathbf{r})$  and the lateral pressure by  $p(\mathbf{r})$ . Assuming that the incompressibility condition holds for the fluid membrane, we write its hydrodynamic equations as

$$\nabla \cdot \mathbf{v} = 0, \quad (4)$$

$$\eta_m \nabla^2 \mathbf{v} - \nabla p + \mathbf{f}_s + \mathbf{F} = 0. \quad (5)$$

The second equation is the 2D Stokes equation, where  $\mathbf{f}_s$  is the force exerted on the membrane by the surrounding solvent, and  $\mathbf{F}$  is any external force acting on the membrane. If we denote the upper and lower solvents with the superscripts  $\pm$ , the two solvent velocities  $\mathbf{v}^\pm(\mathbf{r}, z)$  and pressures  $p^\pm(\mathbf{r}, z)$  obey the following hydrodynamic equations, respectively

$$\hat{\nabla} \cdot \mathbf{v}^\pm = 0, \quad (6)$$

$$\eta_s \hat{\nabla}^2 \mathbf{v}^\pm - \hat{\nabla} p^\pm = 0, \quad (7)$$

where  $\hat{\nabla}$  stands for the 3D differential operator.

The boundary conditions at the membrane are non-slip leading to matching of the membrane and solvent velocities at the membrane plane,  $z = 0$ . Furthermore, the solvent velocity vanishes at the  $z = \pm h$  walls. By solving the above coupled hydrodynamic equations in Fourier space with  $\mathbf{k} = (k_x, k_y)$  being the 2D wavevector, the 2D mobility tensor  $G_{\alpha\beta}(\mathbf{k})$  defined through  $v_\alpha(\mathbf{k}) = G_{\alpha\beta}(\mathbf{k}) F_\beta(\mathbf{k})$  can be obtained as [25–27]

$$G_{\alpha\beta}(\mathbf{k}) = \frac{\delta_{\alpha\beta} - \hat{k}_\alpha \hat{k}_\beta}{\eta_m [k^2 + \nu k \coth(kh)]}, \quad (8)$$

where  $k = |\mathbf{k}|$  and  $\hat{k}_\alpha = k_\alpha/k$ , and the ratio of the two viscosities  $\nu^{-1} = \eta_m/(2\eta_s)$  defines the Saffman-Delbrück (SD) hydrodynamic screening length [4, 5].

In order to perform analytical calculations, the two limiting cases of Eq. (8) are considered, i.e., the “free membrane” case and the “confined membrane” case corresponding to the limits of  $h \rightarrow \infty$  and  $h \rightarrow 0$ , respectively [25–27]. For the free membrane case, we take the limit  $kh \gg 1$  in Eq. (8) and obtain the following asymptotic expression

$$G_{\alpha\beta}^F(\mathbf{k}) = \frac{\delta_{\alpha\beta} - \hat{k}_\alpha \hat{k}_\beta}{\eta_m (k^2 + \nu k)}. \quad (9)$$

Hereafter, we shall denote the quantities for the free membrane case with the superscript “F”. For the confined membrane case, on the other hand, we take the opposite limit  $kh \ll 1$  and obtain

$$G_{\alpha\beta}^C(\mathbf{k}) = \frac{\delta_{\alpha\beta} - \hat{k}_\alpha \hat{k}_\beta}{\eta_m (k^2 + \kappa^2)}, \quad (10)$$

where  $\kappa^{-1} = (h/\nu)^{1/2}$  is the Evans-Sackmann (ES) screening length [7], and we use the superscript “C” for the quantities related to the confined membrane case. We note that the ES screening length  $\kappa^{-1}$  is the geometric mean of  $\nu^{-1}$  and  $h$  so that we typically have  $\kappa^{-1} < \nu^{-1}$ .

Taking the inverse Fourier transform of Eqs. (9) and (10), we obtain the mobility tensors in the real space for the two limiting cases as [25–27]

$$G_{\alpha\beta}^F(\mathbf{r}) = \frac{1}{4\eta_m} \left[ \mathbf{H}_0(\nu r) - Y_0(\nu r) + \frac{2}{\pi \nu^2 r^2} - \frac{\mathbf{H}_1(\nu r)}{\nu r} + \frac{Y_1(\nu r)}{\nu r} \right] \delta_{\alpha\beta} + \frac{1}{4\eta_m} \left[ -\frac{4}{\pi \nu^2 r^2} + \frac{2\mathbf{H}_1(\nu r)}{\nu r} - \frac{2Y_1(\nu r)}{\nu r} - \mathbf{H}_0(\nu r) + Y_0(\nu r) \right] \hat{r}_\alpha \hat{r}_\beta, \quad (11)$$

and

$$G_{\alpha\beta}^C(\mathbf{r}) = \frac{1}{2\pi\eta_m} \left[ K_0(\kappa r) + \frac{K_1(\kappa r)}{\kappa r} - \frac{1}{\kappa^2 r^2} \right] \delta_{\alpha\beta} + \frac{1}{2\pi\eta_m} \left[ -K_0(\kappa r) - \frac{2K_1(\kappa r)}{\kappa r} + \frac{2}{\kappa^2 r^2} \right] \hat{r}_\alpha \hat{r}_\beta, \quad (12)$$

respectively, where we have used the notations  $r = |\mathbf{r}|$  and  $\hat{r}_\alpha = r_\alpha/r$ . In the above,  $\mathbf{H}_n(z)$  are the Struve functions,  $Y_n(z)$  the Bessel functions of the second kind, and  $K_n(z)$  the modified Bessel functions of the second kind. The physical meaning of the above expressions was also discussed in Refs. [31–33]. We note that if there is only one wall instead of two walls, the definition of the ES length needs to be modified as  $\kappa^{-1} \rightarrow (2h/\nu)^{1/2}$  [33]. In the next sections, we shall use Eqs. (11) and (12) to calculate the active diffusion coefficients and the drift velocity.

### III. ACTIVE DIFFUSION COEFFICIENT

#### A. Free membranes

We first calculate the active diffusion coefficient for the free membrane case by substituting Eq. (11) into Eq. (1). Since the integrand in Eq. (1) diverges logarithmically at short distances, we need to introduce a small cutoff length  $\ell_c$ . Physically,  $\ell_c$  can be regarded as the size of a passive particle undergoing a lateral Brownian motion due to active force dipoles. Another interpretation of  $\ell_c$  is provided in Sec. VI.

Introducing a dimensionless vector  $\mathbf{z} = \nu \mathbf{r}$  scaled by the SD length, we can write the active diffusion coefficient for the free membrane case as

$$D_A^F = \frac{Sc_0}{32\pi^2\eta_m^2} \int_{\delta}^{\infty} d^2z \Omega_{\beta\beta'\gamma\gamma'} \frac{\partial g_{\alpha\beta}^F(\mathbf{z})}{\partial z_\gamma} \frac{\partial g_{\alpha\beta'}^F(\mathbf{z})}{\partial z_{\gamma'}}, \quad (13)$$

where  $\delta = \nu\ell_c$  is the dimensionless cutoff, and  $g_{\alpha\beta}^F(\mathbf{z}) = 4\pi\eta_m G_{\alpha\beta}^F$  is the corresponding dimensionless mobility tensor [see Eq. (11)]. We have first evaluated the above integral numerically. In Fig. 2, we plot the obtained  $D_A^F$  as a function of  $\delta = \nu\ell_c$  by the solid line. We see that the active diffusion coefficient depends only weakly on the particle size at small scales, whereas it shows a stronger size dependence described by a power-law behavior at large scales. The crossover between these two behaviors is set by the condition  $\delta \approx 1$ .

In order to understand the above behaviors, we next discuss the asymptotic behaviors of  $D_A^F$  for both small and large  $\delta$  values. Expanding the mobility tensor in Eq. (11) for  $\nu r \ll 1$  and  $\nu r \gg 1$ , we have [33]

$$g_{\alpha\beta}^F(\mathbf{z}) \approx \left( \ln \frac{2}{z} - \gamma - \frac{1}{2} \right) \delta_{\alpha\beta} + \hat{z}_\alpha \hat{z}_\beta, \quad (14)$$

and

$$g_{\alpha\beta}^F(\mathbf{z}) \approx \frac{2}{z} \hat{z}_\alpha \hat{z}_\beta, \quad (15)$$

respectively, where  $\gamma = 0.5722\cdots$  is Euler's constant. By substituting Eqs. (14) and (15) into Eq. (13), we can analytically obtain the asymptotic forms of the active diffusion coefficient as a function of  $\delta = \nu\ell_c$ .

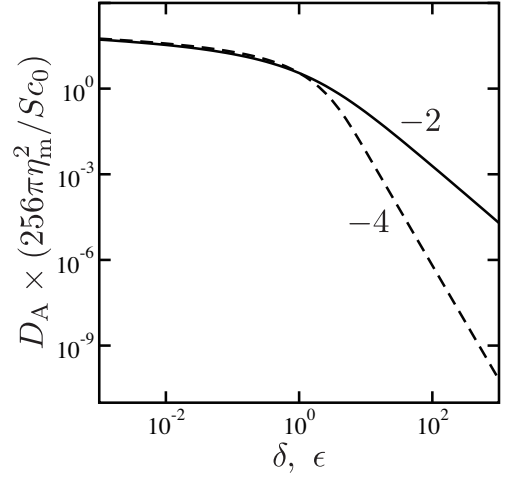


FIG. 2. The plot of the scaled active diffusion coefficient  $D_A$  as a function of the scaled cutoff length  $\delta = \nu\ell_c$  and  $\epsilon = \kappa\ell_c$  for the free membrane case [solid line, see Eq. (13)] and the confined membrane case [dashed line, see Eq. (18)], respectively. Here  $D_A$  is scaled by  $Sc_0/(256\pi\eta_m^2)$ . The numbers in this plot indicate the slope of the curves and represent the powers of the algebraic dependencies.

As obtained in Ref. [19], we find for  $\delta \ll 1$

$$D_A^F \approx \frac{Sc_0}{32\pi\eta_m^2} \ln \frac{L}{\ell_c}, \quad (16)$$

where a large cutoff length  $L$  is introduced because the integral in Eq. (13) also diverges logarithmically at large distances. In order to match with the numerical estimation, we obtain  $L \approx 0.682\nu^{-1}$ . The above logarithmic dependence on  $\ell_c$  means that  $D_A^F$  depends only weakly on the particle size. We also note that the above expression contains only the membrane viscosity  $\eta_m$ , and does not depend on the solvent viscosity  $\eta_s$ . This is because the hydrodynamics at small scales is primarily dominated by the 2D membrane property.

In the opposite limit of  $\delta \gg 1$ , on the other hand, we show in the Appendix A that the active diffusion coefficient becomes

$$D_A^F \approx \frac{5Sc_0}{256\pi\eta_s^2} \frac{1}{\ell_c^2}, \quad (17)$$

which is an important result of this paper. This asymptotic expression decays as  $1/\ell_c^2$  and depends now only on  $\eta_s$ , indicating that the membrane lateral dynamics is governed by the surrounding 3D fluid at large scales. From the obtained asymptotic expressions in Eqs. (16) and (17), the behavior of  $D_A^F$  in Fig. 2 is explained as a crossover from a logarithmic dependence to an algebraic dependence with a power of  $-2$ .



### B. Confined membranes

Next we consider the confined membrane case. With the use of Eq. (12) the active diffusion coefficient can be written as

$$D_A^C = \frac{Sc_0}{32\pi^2\eta_m^2} \int_{\epsilon}^{\infty} d^2w \Omega_{\beta\beta'\gamma\gamma'} \frac{\partial g_{\alpha\beta}^C(\mathbf{w})}{\partial w_{\gamma}} \frac{\partial g_{\alpha\beta'}^C(\mathbf{w})}{\partial w_{\gamma'}}, \quad (18)$$

where  $\mathbf{w} = \kappa\mathbf{r}$  is a different dimensionless variable,  $\epsilon = \kappa\ell_c$  is a differently scaled cutoff, and  $g_{\alpha\beta}^C(\mathbf{w}) = 4\pi\eta_m G_{\alpha\beta}^C$  is the corresponding dimensionless mobility tensor [see Eq. (12)]. Performing the numerical integration of Eq. (18), we plot in Fig. 2 the active diffusion coefficient  $D_A^C$  as a function of  $\epsilon = \kappa\ell_c$  by the dashed line. For small  $\epsilon$  values, the behavior of  $D_A^C$  is similar to that of  $D_A^F$ , while  $D_A^C$  decays much faster than  $D_A^F$  for large  $\epsilon$  values.

To discuss these size dependencies, we use the asymptotic expressions of Eq. (12) for  $\kappa r \ll 1$  and  $\kappa r \gg 1$  given by [33]

$$g_{\alpha\beta}^C(\mathbf{w}) \approx \left( \ln \frac{2}{w} - \gamma - \frac{1}{2} \right) \delta_{\alpha\beta} + \hat{w}_{\alpha} \hat{w}_{\beta}, \quad (19)$$

and

$$g_{\alpha\beta}^C(\mathbf{w}) \approx -\frac{2}{w^2} (\delta_{\alpha\beta} - 2\hat{w}_{\alpha} \hat{w}_{\beta}), \quad (20)$$

respectively. Note that Eq. (19) is identical to Eq. (14) when  $w$  is replaced by  $z$ . Hence, in the limit of  $\epsilon \ll 1$ , the active diffusion coefficient for the confined membrane case should be identical to Eq. (16) and is given by [19]

$$D_A^C \approx \frac{Sc_0}{32\pi\eta_m^2} \ln \frac{L}{\ell_c}. \quad (21)$$

The large cutoff length should be taken here as  $L \approx 1.12\kappa^{-1}$ . As mentioned before, the 2D hydrodynamic effect is more important at small scales, and  $D_A^C$  is logarithmically dependent on the particle size.

In the large size limit of  $\epsilon \gg 1$ , on the other hand, we also show in the Appendix A that  $D_A^C$  asymptotically behaves as

$$D_A^C \approx \frac{Sc_0}{16\pi\eta_s^2} \frac{h^2}{\ell_c^4}, \quad (22)$$

which is another important result. The obtained expression decays as  $1/\ell_c^4$  which is much stronger than Eq. (17) for the free membrane case. According to Eqs. (21) and (22), the behavior of  $D_A^C$  in Fig. 2 can be understood as a crossover from a logarithmic dependence to an algebraic dependence with a power of  $-4$ .

## IV. TOTAL DIFFUSION COEFFICIENT

Having obtained the active diffusion coefficients for the free and the confined membrane cases, we now discuss

the total lateral diffusion coefficients in membranes by considering both thermal and non-thermal contributions. Concerning the thermal diffusion coefficient  $D_T^F$  for the free membrane case, we use an empirical expression obtained by Petrov and Schville [34, 35]

$$D_T^F(\delta) = \frac{k_B T}{4\pi\eta_m} \left[ \ln \frac{2}{\delta} - \gamma + \frac{4\delta}{\pi} - \frac{\delta^2}{2} \ln \frac{2}{\delta} \right] \times \left[ 1 - \frac{\delta^3}{\pi} \ln \frac{2}{\delta} + \frac{c_1 \delta^{b_1}}{1 + c_2 \delta^{b_2}} \right]^{-1}, \quad (23)$$

where  $k_B$  is the Boltzmann constant,  $T$  is the temperature, and the four numerical constants are chosen as  $c_1 = 0.73761$ ,  $b_1 = 2.74819$ ,  $c_2 = 0.52119$ , and  $b_2 = 0.51465$  [35]. For the free membrane case, there is no exact analytical expression of the thermal diffusion coefficient which covers the entire size range, except for the case where a 2D polymer chain is confined in a fluid membrane [25]. Equation (23) is known to recover the correct asymptotic limits of the thermal diffusion coefficients both for  $\delta \ll 1$  [4, 5] and  $\delta \gg 1$  [6].

On the other hand, the thermal diffusion coefficient  $D_T^C$  for the confined membrane case was explicitly calculated by Evans *et al.* [7] and also by Ramachandran *et al.* [8–11]. In this case, the resulting expression is given by

$$D_T^C(\epsilon) = \frac{k_B T}{4\pi\eta_m} \left[ \frac{\epsilon^2}{4} + \frac{\epsilon K_1(\epsilon)}{K_0(\epsilon)} \right]^{-1}. \quad (24)$$

In Fig. 3, we plot  $D_T^F$  as a function of the particle size  $\delta$  by the solid line, and  $D_T^C$  as a function of  $\epsilon$  by the dashed line for the whole size range. Their asymptotic behaviors are separately discussed below.

### A. Free membranes

For the free membrane case, the total diffusion coefficient is given by  $D^F = D_T^F + D_A^F$ , where the active non-thermal contribution  $D_A^F$  was discussed in the previous section. Using Eqs. (23) and (16) in the limit of  $\delta \ll 1$ , we asymptotically have [4, 5]

$$D^F \approx \frac{k_B T}{4\pi\eta_m} \left( \ln \frac{2}{\nu\ell_c} - \gamma \right) + \frac{Sc_0}{32\pi\eta_m^2} \ln \frac{L}{\ell_c}, \quad (25)$$

where both contributions are proportional to  $\ln(1/\ell_c)$ .

For  $\delta \gg 1$ , on the other hand, we obtain from Eqs. (23) and (17) [6]

$$D^F \approx \frac{k_B T}{16\eta_s} \frac{1}{\ell_c} + \frac{5Sc_0}{256\pi\eta_s^2} \frac{1}{\ell_c^2}. \quad (26)$$

Since the  $\ell_c$ -dependencies in Eq. (26) are different between the thermal and non-thermal contributions, we can introduce a new crossover length defined by

$$\ell^* = \frac{5Sc_0}{16\pi k_B T \eta_s}. \quad (27)$$

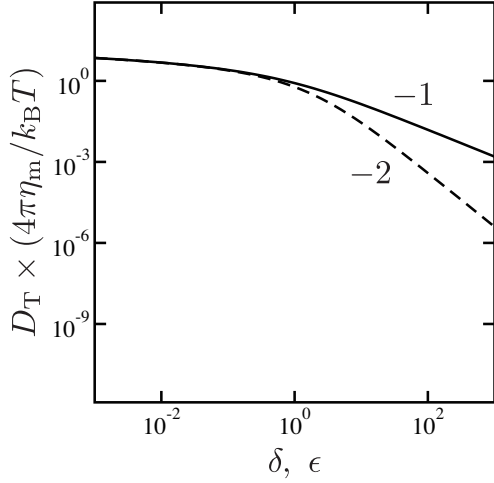


FIG. 3. The plot of the scaled thermal diffusion coefficient  $D_T$  as a function of the scaled cutoff length  $\delta = \nu\ell_c$  and  $\epsilon = \kappa\ell_c$  for the free membrane case [solid line, see Eq. (23)] and the confined membrane case [dashed line, see Eq. (24)], respectively. Here  $D_T$  is scaled by  $k_B T / (4\pi\eta_m)$ . The numbers in this plot indicate the slope of the curves and represent the powers of the algebraic dependencies.

This length scale characterizes a crossover from the  $1/\ell_c^2$ -dependence to  $1/\ell_c$ -dependence. When  $\ell_c \ll \ell^*$  (but still  $\nu^{-1} \ll \ell_c$ ), the non-thermal contribution dominates over the thermal one, while in the opposite limit of  $\ell_c \gg \ell^*$ , the thermal contribution is of primary importance.

### B. Confined membranes

In the case of confined membranes, the total diffusion coefficient now becomes  $D^C = D_T^C + D_A^C$ . In the limit of  $\epsilon \ll 1$ , we have from Eqs. (24) and (21) [7, 8]

$$D^C \approx \frac{k_B T}{4\pi\eta_m} \left( \ln \frac{2}{\kappa\ell_c} - \gamma \right) + \frac{Sc_0}{32\pi\eta_m^2} \ln \frac{L}{\ell_c}, \quad (28)$$

where both contributions exhibit a logarithmic dependence on  $\ell_c$  as in the free membrane case.

In the opposite limit of  $\epsilon \gg 1$ , we find from Eqs. (24) and (22) [7, 8]

$$D^C \approx \frac{k_B T}{2\pi\eta_s} \frac{h}{\ell_c^2} + \frac{Sc_0}{16\pi\eta_s^2} \frac{h^2}{\ell_c^4}. \quad (29)$$

Similar to the free membrane case, we can consider another characteristic length defined by

$$\ell^{**} = \left( \frac{Sc_0 h}{8k_B T \eta_s} \right)^{1/2}. \quad (30)$$

This length scale characterizes a crossover from the  $1/\ell_c^4$ -dependence to  $1/\ell_c^2$ -dependence. We note that  $\ell^{**}$  is essentially the geometric mean of  $\ell^*$  and  $h$ . Numerical estimates of these two characteristic length scales will be discussed in Sec. VI.

## V. DRIFT VELOCITY

### A. Free membranes

In this section, we calculate the drift velocity  $V$  of a passive particle due to a concentration gradient of active force dipoles. For the free membrane case, we substitute Eq. (11) into Eq. (3) and obtain

$$V^F = - \frac{S|\nabla c|}{16\pi^2\eta_m^2} \int_{\delta}^{\infty} d^2z \Omega_{\beta\beta'\gamma\gamma'} \times \hat{n}_{\alpha} \frac{\partial^2 g_{\alpha\beta}^F(\mathbf{z})}{\partial z_{\gamma} \partial z_{\delta}} \frac{\partial g_{\delta\beta'}^F(\mathbf{z})}{\partial z_{\gamma'}} (\mathbf{z} \cdot \hat{\mathbf{n}}), \quad (31)$$

where  $\delta = \nu\ell_c$  and  $g_{\alpha\beta}^F(\mathbf{z}) = 4\pi\eta_m G_{\alpha\beta}^F$  as before. Performing the numerical integration of Eq. (31), we plot in Fig. 4 the drift velocity  $V^F$  as a function of  $\delta$  by the solid line. Similar to the active diffusion coefficient  $D_A^F$ , the drift velocity  $V^F$  depends weakly on the particle size at small scales, while it exhibits a stronger size dependence at large scales. Such a crossover also occurs around  $\delta \approx 1$ .

We next discuss the asymptotic behaviors of  $V^F$  for small and large  $\delta$  values. With the use of Eqs. (14) and (15), we show in the Appendix B that the asymptotic behaviors of  $V$  for  $\delta \ll 1$  and  $\delta \gg 1$  are

$$V^F \approx \frac{S|\nabla c|}{32\pi\eta_m^2} \ln \frac{L}{\ell_c}, \quad (32)$$

and

$$V^F \approx \frac{13S|\nabla c|}{256\pi\eta_s^2} \frac{1}{\ell_c^2}, \quad (33)$$

respectively, where we choose  $L \approx 1.85\nu^{-1}$ . Note that Eq. (32) was previously derived in Ref. [19] for a 2D membrane, while Eq. (33) is a new result. As we see in Eqs. (32) and (33), there is a crossover from a logarithmic to an algebraic dependence with a power of  $-2$  when  $\delta$  is increased. These behaviors are consistent with the numerical plot in Fig. 4 for the free membrane case.

### B. Confined membranes

Finally we calculate the drift velocity for the confined membrane case. Substituting Eq. (12) into Eq. (3), we now obtain

$$V^C = - \frac{S|\nabla c|}{16\pi^2\eta_m^2} \int_{\epsilon}^{\infty} d^2w \Omega_{\beta\beta'\gamma\gamma'} \times \hat{n}_{\alpha} \frac{\partial^2 g_{\alpha\beta}^C(\mathbf{w})}{\partial w_{\gamma} \partial w_{\delta}} \frac{\partial g_{\delta\beta'}^C(\mathbf{w})}{\partial w_{\gamma'}} (\mathbf{w} \cdot \hat{\mathbf{n}}), \quad (34)$$

where  $\epsilon = \kappa\ell_c$  and  $g_{\alpha\beta}^C(\mathbf{w}) = 4\pi\eta_m G_{\alpha\beta}^C$  as before. In Fig. 4, we present numerically calculated  $V^C$  as a function of  $\epsilon$  by the dashed line. As  $\epsilon$  is increased, we see a

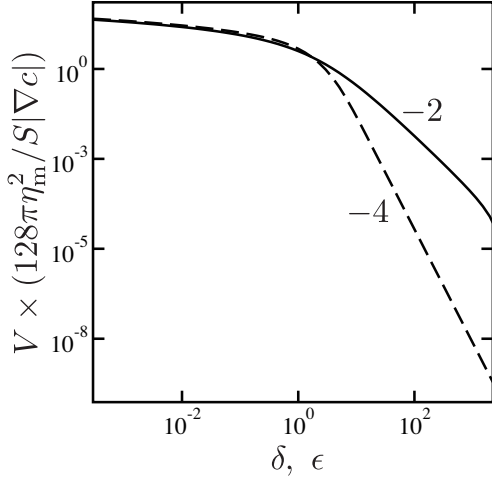


FIG. 4. The plot of the scaled drift velocity  $V$  as a function of the scaled cutoff length  $\delta = \nu\ell_c$  and  $\epsilon = \kappa\ell_c$  for the free membrane case [solid line, see Eq. (31)] and the confined membrane case [dashed line, see Eq. (34)], respectively. Here  $V$  is scaled by  $S|\nabla c|/(128\pi\eta_m^2)$ . The numbers in this plot indicate the slope of the curves and represent the powers of the algebraic dependencies.

crossover from a logarithmic to an algebraic dependence, although  $V^C$  decays faster than  $V^F$  at large scales.

The asymptotic behaviors of  $V^C$  for small and large  $\epsilon$  values can be discussed similarly. Using Eqs. (19) and (20), we obtain in the Appendix B the asymptotic expressions of  $V^C$  for  $\epsilon \ll 1$  and  $\epsilon \gg 1$  as

$$V^C \approx \frac{S|\nabla c|}{32\pi\eta_m^2} \ln \frac{L}{\ell_c}, \quad (35)$$

and

$$V^C \approx \frac{3S|\nabla c|}{16\pi\eta_s^2} \frac{h^2}{\ell_c^4}, \quad (36)$$

respectively, and we choose  $L \approx 3.05\kappa^{-1}$  to coincide with the numerical integration. We note that Eqs. (32) and (35) are identical and depend only on  $\eta_m$  for small sizes [19].

From Fig. 4 and Eqs. (32), (33), (35) and (36), we see that the drift velocity  $V$  is always positive. This means that passive particles move toward higher concentrations of active proteins, and a chemotaxis-like drift takes place in the presence of protein concentration gradients [19–21]. The dominant viscosity dependence of  $V$  switches from  $\eta_m$  to  $\eta_s$  as the particle size exceeds the corresponding hydrodynamic screening length, namely,  $\nu^{-1}$  or  $\kappa^{-1}$ .

## VI. SUMMARY AND DISCUSSION

In this paper, we have investigated lateral diffusion induced by active force dipoles embedded in a biomembrane. In particular, we have calculated the active diffusion coefficient and the drift velocity for the free and

the confined membrane cases by taking into account the hydrodynamic coupling between the membrane and the surrounding bulk solvent. The force dipole model in Refs. [19, 20] and the general membrane mobility tensors obtained in Refs. [25–27] have been employed in our work. When the size of a passive diffusing particle is small, the active diffusion coefficients for the free and the confined membranes represent the same logarithmic size dependence, as shown in Eqs. (16) and (21), respectively [19]. In the opposite large size limit, we find algebraic dependencies with powers  $-2$  and  $-4$  for the two cases, as given by Eqs. (17) and (22), respectively. These are the important outcomes of this paper and are also summarized in Table I together with other asymptotic expressions.

In our work, we have assumed that the total diffusion coefficient is provided by the sum of thermal and non-thermal contributions. For small particle sizes, we have shown that both the total  $D^F$  and  $D^C$  exhibit a logarithmic size dependence [19], whereas different contributions have different size dependencies for large particle sizes. From this result, we have obtained two characteristic length scales that describe the crossover from non-thermal to thermal behaviors when the particle size is larger than the hydrodynamic screening length. The drift velocity in the presence of a concentration gradient of active proteins exhibits the same size dependencies as the active diffusion coefficient for the two membrane geometries.

Here we give some numerical estimates of the obtained crossover length scales. Using typical values such as  $k_B T \approx 4 \times 10^{-21}$  J,  $\eta_s \approx 10^{-3}$  Pa·s,  $h \approx 10^{-9}$  m,  $S \approx 10^{-42}$  J<sup>2</sup>·s, and  $c_0 \approx 10^{14}$  m<sup>-2</sup> [19], we obtain  $\ell^* \approx 2 \times 10^{-6}$  m [see Eq. (27)] and  $\ell^{**} \approx 6 \times 10^{-8}$  m [see Eq. (30)]. On the other hand, the SD and the ES screening lengths are typically  $\nu^{-1} \approx 5 \times 10^{-7}$  m and  $\kappa^{-1} \approx 2 \times 10^{-8}$  m, respectively [4, 5, 7, 8]. Hence  $\ell^*$  and  $\ell^{**}$  are typically larger than  $\nu^{-1}$  and  $\kappa^{-1}$ , respectively. Moreover, the values of  $S$  and  $c_0$  can vary significantly in one membrane to another as pointed out in Ref. [19]. For example, when active proteins are confined in raft domains [28–30], the 2D concentration  $c_0$  can be much larger. Therefore, one or two orders of magnitude changes of  $S$  or  $c_0$  are possible. If  $\ell^*$  and  $\ell^{**}$  are much larger than the screening lengths  $\nu^{-1}$  and  $\kappa^{-1}$ , respectively, the three different scaling regimes of the total diffusion coefficient are expected as the particle size is increased, i.e.,  $\ln(1/\ell_c) \rightarrow 1/\ell_c^2 \rightarrow 1/\ell_c$  for the free membrane case, and  $\ln(1/\ell_c) \rightarrow 1/\ell_c^4 \rightarrow 1/\ell_c^2$  for the confined membrane case.

Momentum in a membrane is conserved over distances smaller than the hydrodynamic screening length (either  $\nu^{-1}$  or  $\kappa^{-1}$ ), whereas it leaks to the surrounding fluid beyond that length scale [31–33]. Within a membrane, the velocity decays as  $\ln(1/r)$  at short distances, as shown in Eqs. (14) and (19), due to the momentum conservation in 2D. These 2D behaviors also lead to the logarithmic dependence of the active diffusion coefficients in Eqs. (16)

TABLE I. Summary of the asymptotic dependencies of the thermal diffusion coefficient  $D_T$ , the active diffusion coefficient  $D_A$ , and the drift velocity  $V$  on the passive particle size  $\ell_c$ . The numbers after the asymptotic expressions correspond to the equation numbers in this paper.

cases	limits	$D_T$	$D_A$	$V$
free membrane	$\nu\ell_c \ll 1$	$\ln(1/\ell_c)$ (25)	$\ln(1/\ell_c)$ (16)	$\ln(1/\ell_c)$ (32)
$(hk \gg 1)$	$\nu\ell_c \gg 1$	$1/\ell_c$ (26)	$1/\ell_c^2$ (17)	$1/\ell_c^2$ (33)
confined membrane	$\kappa\ell_c \ll 1$	$\ln(1/\ell_c)$ (28)	$\ln(1/\ell_c)$ (21)	$\ln(1/\ell_c)$ (35)
$(hk \ll 1)$	$\kappa\ell_c \gg 1$	$1/\ell_c^2$ (29)	$1/\ell_c^4$ (22)	$1/\ell_c^4$ (36)

and (21). For the free membrane case, the velocity decays as  $1/r$  at large scales as shown in Eq. (15) due to the momentum conservation in the 3D bulk. This behavior is reflected in the first term of Eq. (26) for the thermal diffusion coefficient [6]. As shown in Eq. (20), however, the velocity decays as  $1/r^2$  at large scales for the confined membrane case. This behavior essentially arises from the mass conservation in 2D while the total momentum is not conserved due to the presence of the walls which break the translational symmetry of the system [31–33]. The corresponding contribution is the first term of Eq. (29) for the thermal diffusion coefficient [7, 8].

In Sec. III, we mentioned that the small cutoff length  $\ell_c$  in the integrals physically corresponds to the size of a passive particle. An alternative way to interpret this length scale is to consider a flow velocity tracer which can be introduced by choosing a certain volume element of the 2D fluid membrane and following its motion with time [14, 15]. The flow velocity tracers can only follow those velocity fluctuations whose characteristic length scale is larger than the tracer size  $\ell_c$ . Hence, they visualize the coarse-grained fluctuating fields obtained by averaging over the area elements of linear size  $\ell_c$ . Such fluctuating fields include only the contributions from spatial Fourier modes with wavelength larger than  $\ell_c$ .

The active diffusion coefficient  $D_A^F$  obtained in Eq. (17) for the free membrane case essentially reflects the hydrodynamics of the surrounding bulk 3D solvent. Hence our result can be compared with that in Ref. [19] obtained for a purely 3D fluid system:

$$D_A^{3D} \approx \frac{Sc_0^{3D}}{60\pi\eta_s^2} \frac{1}{\ell_c}, \quad (37)$$

which decays as  $1/\ell_c$  and is different from Eq. (17). In fact, such a difference arises from the different dimensions of the dipole concentrations, i.e.,  $c_0$  is the 2D concentration in our case, while  $c_0^{3D}$  is the 3D concentration in Ref. [19]. A similar comparison can be also made for the drift velocity of free membranes in Eq. (33) and that in Ref. [19] for a 3D fluid system:

$$V^{3D} \approx \frac{S|\nabla c^{3D}|}{30\pi\eta_s^2} \frac{1}{\ell_c}. \quad (38)$$

The same reason holds for the different  $\ell_c$ -dependence.

At this stage, we also comment that both the active diffusion coefficient  $D_A$  and the drift velocity  $V$  exhibit the

same  $\ell_c$ -dependence. Although the integrands in Eqs. (1) and (3) look apparently different, their physical dimensions are identical because the first derivative of the mobility tensor in Eq. (1) corresponds to the product of the second derivative and  $(\mathbf{r} \cdot \hat{\mathbf{n}})$  in Eq. (3). This is the simple reason that they exhibit the same  $\ell_c$ -dependence. One can also easily confirm that  $V$  is positive when we make use of the membrane mobility tensor, because the integrand in Eq. (3) is the product of the first and the second derivatives of the mobility tensor which have opposite signs. This leads to  $V > 0$  indicating a chemotaxis-like drift as mentioned before.

In this work, we have assumed that active proteins generate forces only in the lateral directions. On the other hand, actual active motors such as bacteriorhodopsin can also exert forces to the surrounding solvent [16–18]. Although we did not take into account such normal forces which induce membrane undulation, consideration of normal forces as well as lateral ones will provide us with a general understanding of active diffusion in biomembranes [36].

We have also assumed that the force dipoles are fixed in a membrane and are distributed homogeneously. It would be interesting to consider the case when active proteins can also move laterally in the membrane and even interact with each other through a nematic-like interaction. Then one needs to introduce a free energy which describes the spatial inhomogeneity of force dipoles and their interactions [37]. The dynamics of the dipole concentration should be essentially determined by a diffusion equation under the external force that is determined by the free energy. However, not only thermal diffusion of active proteins, but also their active non-thermal diffusion should be taken into account. Our work is the first step toward such a full description of very rich biomembrane dynamics.

## ACKNOWLEDGMENTS

We thank A. S. Mikhailov and T. Kato for useful discussions. S.K. and R.O. acknowledge support from the Grant-in-Aid for Scientific Research on Innovative Areas “*Fluctuation and Structure*” (Grant No. 25103010) from the Ministry of Education, Culture, Sports, Science, and Technology of Japan, and the Grant-in-Aid for Scientific



Research (C) (Grant No. 15K05250) from the Japan Society for the Promotion of Science (JSPS).

### Appendix A: Derivation of Eqs. (17) and (22)

Since Eqs. (16) and (21) have been obtained in Ref. [19], we show here the derivation of Eqs. (17) and (22). Substituting Eq. (15) into Eq. (13), we get

$$D_A^F = \frac{Sc_0}{8\pi^2\eta_m^2} \int_{\delta}^{\infty} d^2z \Omega_{\beta\beta'\gamma\gamma'} \times \frac{\partial}{\partial z_{\gamma}} \left( \frac{\hat{z}_{\alpha}\hat{z}_{\beta}}{z} \right) \frac{\partial}{\partial z_{\gamma'}} \left( \frac{\hat{z}_{\alpha}\hat{z}_{\beta'}}{z} \right), \quad (A1)$$

where  $\mathbf{z} = \nu\mathbf{r}$ . Since

$$\frac{\partial}{\partial z_{\gamma}} \left( \frac{\hat{z}_{\alpha}\hat{z}_{\beta}}{z} \right) = \frac{1}{z^3} (\delta_{\alpha\gamma}z_{\beta} + \delta_{\beta\gamma}z_{\alpha}) - \frac{3}{z^5} z_{\alpha}z_{\beta}z_{\gamma}, \quad (A2)$$

the integrand in Eq. (A1) becomes

$$\begin{aligned} & \frac{\partial}{\partial z_{\gamma}} \left( \frac{\hat{z}_{\alpha}\hat{z}_{\beta}}{z} \right) \frac{\partial}{\partial z_{\gamma'}} \left( \frac{\hat{z}_{\alpha}\hat{z}_{\beta'}}{z} \right) = \frac{1}{z^4} \delta_{\beta\gamma} \delta_{\beta'\gamma'} \\ & + \frac{1}{z^6} [\delta_{\gamma\gamma'} z_{\beta} z_{\beta'} - 2(\delta_{\beta\gamma} z_{\beta'} z_{\gamma'} + \delta_{\beta'\gamma'} z_{\beta} z_{\gamma})] \\ & + \frac{3}{z^8} z_{\beta} z_{\beta'} z_{\gamma} z_{\gamma'}. \end{aligned} \quad (A3)$$

By operating  $\Omega_{\beta\beta'\gamma\gamma'}$ , we have

$$\Omega_{\beta\beta'\gamma\gamma'} \frac{\partial}{\partial z_{\gamma}} \left( \frac{\hat{z}_{\alpha}\hat{z}_{\beta}}{z} \right) \frac{\partial}{\partial z_{\gamma'}} \left( \frac{\hat{z}_{\alpha}\hat{z}_{\beta'}}{z} \right) = \frac{5}{8z^4}. \quad (A4)$$

After the integration, we obtain Eq. (17).

Similarly, we substitute Eq. (20) into Eq. (18) and obtain

$$D_A^C = \frac{Sc_0}{8\pi^2\eta_m^2} \int_{\epsilon}^{\infty} d^2w \Omega_{\beta\beta'\gamma\gamma'} \times \frac{\partial}{\partial w_{\gamma}} \left( \frac{\delta_{\alpha\beta} - 2\hat{w}_{\alpha}\hat{w}_{\beta}}{w^2} \right) \frac{\partial}{\partial w_{\gamma'}} \left( \frac{\delta_{\alpha\beta'} - 2\hat{w}_{\alpha}\hat{w}_{\beta'}}{w^2} \right), \quad (A5)$$

where  $\mathbf{w} = \kappa\mathbf{r}$ . Since

$$\begin{aligned} & \frac{\partial}{\partial w_{\gamma}} \left( \frac{\delta_{\alpha\beta} - 2\hat{w}_{\alpha}\hat{w}_{\beta}}{w^2} \right) \\ & = -\frac{2}{w^4} (\delta_{\alpha\beta} w_{\gamma} + \delta_{\beta\gamma} w_{\alpha} + \delta_{\alpha\gamma} w_{\beta}) + \frac{8}{w^6} w_{\alpha} w_{\beta} w_{\gamma}, \end{aligned} \quad (A6)$$

we obtain

$$\begin{aligned} & \frac{\partial}{\partial w_{\gamma}} \left( \frac{\delta_{\alpha\beta} - 2\hat{w}_{\alpha}\hat{w}_{\beta}}{w^2} \right) \frac{\partial}{\partial w_{\gamma'}} \left( \frac{\delta_{\alpha\beta'} - 2\hat{w}_{\alpha}\hat{w}_{\beta'}}{w^2} \right) \\ & = \frac{4}{w^6} \delta_{\beta\gamma} \delta_{\beta'\gamma'} + \frac{4}{w^8} [\delta_{\beta\beta'} w_{\gamma} w_{\gamma'} + \delta_{\beta'\gamma} w_{\beta} w_{\gamma'} + \delta_{\beta\gamma'} w_{\beta'} w_{\gamma} \\ & + \delta_{\gamma\gamma'} w_{\beta} w_{\beta'} - 2(\delta_{\beta\gamma} w_{\beta'} w_{\gamma'} + \delta_{\beta'\gamma'} w_{\beta} w_{\gamma})]. \end{aligned} \quad (A7)$$

By operating  $\Omega_{\beta\beta'\gamma\gamma'}$ , we have

$$\begin{aligned} & \Omega_{\beta\beta'\gamma\gamma'} \frac{\partial}{\partial w_{\gamma}} \left( \frac{\delta_{\alpha\beta} - 2\hat{w}_{\alpha}\hat{w}_{\beta}}{w^2} \right) \frac{\partial}{\partial w_{\gamma'}} \left( \frac{\delta_{\alpha\beta'} - 2\hat{w}_{\alpha}\hat{w}_{\beta'}}{w^2} \right) \\ & = \frac{4}{w^6}. \end{aligned} \quad (A8)$$

After the integration, we obtain Eq. (22).

### Appendix B: Derivation of Eqs. (33) and (36)

In this Appendix, we show the derivation of Eqs. (33) and (36). Substituting Eq. (15) into Eq. (31), we obtain

$$\begin{aligned} V^F &= -\frac{S|\nabla c|}{4\pi^2\eta_m^2} \int_{\delta}^{\infty} d^2z \Omega_{\beta\beta'\gamma\gamma'} \hat{n}_{\alpha} \\ & \times \frac{\partial^2}{\partial z_{\gamma} \partial z_{\delta}} \left( \frac{\hat{z}_{\alpha}\hat{z}_{\beta}}{z} \right) \frac{\partial}{\partial z_{\gamma'}} \left( \frac{\hat{z}_{\delta}\hat{z}_{\beta'}}{z} \right) (\mathbf{z} \cdot \hat{\mathbf{n}}). \end{aligned} \quad (B1)$$

In the above, the derivatives are

$$\begin{aligned} & \frac{\partial^2}{\partial z_{\gamma} \partial z_{\delta}} \left( \frac{\hat{z}_{\alpha}\hat{z}_{\beta}}{z} \right) = \frac{1}{z^3} (\delta_{\alpha\delta} \delta_{\beta\gamma} + \delta_{\alpha\gamma} \delta_{\beta\delta}) \\ & - \frac{3}{z^5} (\delta_{\alpha\delta} z_{\beta} z_{\gamma} + \delta_{\beta\delta} z_{\alpha} z_{\gamma} + \delta_{\alpha\gamma} z_{\beta} z_{\delta} + \delta_{\beta\gamma} z_{\alpha} z_{\delta} \\ & + \delta_{\gamma\delta} z_{\alpha} z_{\beta}) + \frac{15}{z^7} z_{\alpha} z_{\beta} z_{\gamma} z_{\delta}, \end{aligned} \quad (B2)$$

and

$$\begin{aligned} & \frac{\partial^2}{\partial z_{\gamma} \partial z_{\delta}} \left( \frac{\hat{z}_{\alpha}\hat{z}_{\beta}}{z} \right) \frac{\partial}{\partial z_{\gamma'}} \left( \frac{\hat{z}_{\delta}\hat{z}_{\beta'}}{z} \right) \\ & = -\frac{1}{z^6} [2\delta_{\beta'\gamma'} (\delta_{\alpha\gamma} z_{\beta} + \delta_{\beta\gamma} z_{\alpha}) - (\delta_{\alpha\gamma'} \delta_{\beta\gamma} + \delta_{\alpha\gamma} \delta_{\beta'\gamma'}) z_{\beta'}] \\ & - \frac{3}{z^8} [(\delta_{\alpha\gamma'} z_{\beta} z_{\gamma} + \delta_{\beta\gamma'} z_{\alpha} z_{\gamma} - \delta_{\alpha\gamma} z_{\beta} z_{\gamma'} - \delta_{\beta\gamma} z_{\alpha} z_{\gamma'} \\ & + \delta_{\gamma\gamma'} z_{\alpha} z_{\beta}) z_{\beta'} - 2\delta_{\beta'\gamma'} z_{\alpha} z_{\beta} z_{\gamma}] \\ & - \frac{3}{z^{10}} z_{\alpha} z_{\beta} z_{\beta'} z_{\gamma} z_{\gamma'}. \end{aligned} \quad (B3)$$

By operating  $\Omega_{\beta\beta'\gamma\gamma'}$ , we have

$$\Omega_{\beta\beta'\gamma\gamma'} \frac{\partial^2}{\partial z_{\gamma} \partial z_{\delta}} \left( \frac{\hat{z}_{\alpha}\hat{z}_{\beta}}{z} \right) \frac{\partial}{\partial z_{\gamma'}} \left( \frac{\hat{z}_{\delta}\hat{z}_{\beta'}}{z} \right) = -\frac{13z_{\alpha}}{8z^6}. \quad (B4)$$

After the integration, we obtain Eq. (33).

Next we substitute Eq. (20) into Eq. (34) and find

$$\begin{aligned} V^C &= -\frac{S|\nabla c|}{4\pi^2\eta_m^2} \int_{\epsilon}^{\infty} d^2w \Omega_{\beta\beta'\gamma\gamma'} \hat{n}_{\alpha} \\ & \times \frac{\partial^2}{\partial w_{\gamma} \partial w_{\delta}} \left( \frac{\delta_{\alpha\beta} - 2\hat{w}_{\alpha}\hat{w}_{\beta}}{w^2} \right) \\ & \times \frac{\partial}{\partial w_{\gamma'}} \left( \frac{\delta_{\delta\beta'} - 2\hat{w}_{\delta}\hat{w}_{\beta'}}{w^2} \right) (\mathbf{w} \cdot \hat{\mathbf{n}}). \end{aligned} \quad (B5)$$

Here the derivatives are

$$\begin{aligned}
& \frac{\partial^2}{\partial w_\gamma \partial w_\delta} \left( \frac{\delta_{\alpha\beta} - 2\hat{w}_\alpha \hat{w}_\beta}{w^2} \right) \\
&= -\frac{2}{w^4} (\delta_{\alpha\beta} \delta_{\gamma\delta} + \delta_{\alpha\gamma} \delta_{\beta\delta} + \delta_{\alpha\delta} \delta_{\beta\gamma}) \\
&+ \frac{8}{w^6} (\delta_{\alpha\beta} w_\gamma w_\delta + \delta_{\beta\delta} w_\alpha w_\gamma + \delta_{\alpha\delta} w_\beta w_\gamma + \delta_{\alpha\gamma} w_\beta w_\delta \\
&+ \delta_{\beta\gamma} w_\alpha w_\delta + \delta_{\gamma\delta} w_\alpha w_\beta) - \frac{48}{w^8} w_\alpha w_\beta w_\gamma w_\delta, \quad (B6)
\end{aligned}$$

and

$$\begin{aligned}
& \frac{\partial^2}{\partial w_\gamma \partial w_\delta} \left( \frac{\delta_{\alpha\beta} - 2\hat{w}_\alpha \hat{w}_\beta}{w^2} \right) \frac{\partial}{\partial w_{\gamma'}} \left( \frac{\delta_{\delta\beta'} - 2\hat{w}_\delta \hat{w}_{\beta'}}{w^2} \right) \\
&= -\frac{4}{w^8} [3\delta_{\beta'\gamma'} (\delta_{\alpha\beta} w_\gamma + \delta_{\alpha\gamma} w_\beta + \delta_{\beta\gamma} w_\alpha) \\
&- (\delta_{\alpha\beta} \delta_{\gamma\beta'} + \delta_{\alpha\gamma} \delta_{\beta\beta'} + \delta_{\alpha\beta'} \delta_{\beta\gamma}) w_{\gamma'} \\
&- (\delta_{\alpha\beta} \delta_{\gamma\gamma'} + \delta_{\alpha\gamma} \delta_{\beta\gamma'} + \delta_{\alpha\gamma'} \delta_{\beta\gamma}) w_{\beta'}] \\
&+ \frac{16}{w^{10}} [(\delta_{\alpha\beta} w_{\beta'} w_\gamma - \delta_{\beta\beta'} w_\alpha w_\gamma - \delta_{\alpha\beta'} w_\beta w_\gamma \\
&+ \delta_{\alpha\gamma} w_\beta w_{\beta'} + \delta_{\beta\gamma} w_\alpha w_{\beta'} - \delta_{\beta'\gamma} w_\alpha w_\beta) w_{\gamma'} \\
&- (\delta_{\beta\gamma'} w_\alpha w_\gamma + \delta_{\alpha\gamma'} w_\beta w_\gamma + \delta_{\gamma\gamma'} w_\alpha w_\beta) w_{\beta'} \\
&+ 3\delta_{\beta'\gamma'} w_\alpha w_\beta w_\gamma]. \quad (B7)
\end{aligned}$$

By operating  $\Omega_{\beta\beta'\gamma\gamma'}$ , we find

$$\begin{aligned}
& \Omega_{\beta\beta'\gamma\gamma'} \frac{\partial^2}{\partial w_\gamma \partial w_\delta} \left( \frac{\delta_{\alpha\beta} - 2\hat{w}_\alpha \hat{w}_\beta}{w^2} \right) \\
&\times \frac{\partial}{\partial w_{\gamma'}} \left( \frac{\delta_{\delta\beta'} - 2\hat{w}_\delta \hat{w}_{\beta'}}{w^2} \right) = -\frac{12w_\alpha}{w^8}. \quad (B8)
\end{aligned}$$

After the integration, we obtain Eq. (36).

- 
- [1] S. J. Singer and G. L. Nicolson, *Science* **175**, 720 (1972).
  - [2] B. Alberts, A. Johnson, P. Walter, J. Lewis, and M. Raff, *Molecular Biology of the Cell* (Garland Science, New York, 2008).
  - [3] R. Lipowsky and E. Sackmann, *Structure and Dynamics of Membranes* (Elsevier, Amsterdam, 1995).
  - [4] P. G. Saffman and M. Delbrück, *Proc. Natl. Acad. Sci. USA* **72**, 3111 (1975).
  - [5] P. G. Saffman, *J. Fluid Mech.* **73**, 593 (1976).
  - [6] B. D. Hughes, B. A. Pailthorpe, and L.R. White, *J. Fluid Mech.* **110**, 349 (1981).
  - [7] E. Evans and E. Sackmann, *J. Fluid Mech.* **194**, 553 (1988).
  - [8] S. Ramachandran, S. Komura, M. Imai, and K. Seki, *Eur. Phys. J. E* **31**, 303-310 (2010).
  - [9] K. Seki, S. Ramachandran, and S. Komura, *Phys. Rev. E* **84**, 021905 (2011).
  - [10] K. Seki, S. Mogre, and S. Komura, *Phys. Rev. E* **89**, 022713 (2014).
  - [11] S. Komura, S. Ramachandran, and M. Imai, in *Non-Equilibrium Soft Matter Physics*, edited by S. Komura and T. Ohta (World Scientific, Singapore, 2012), p. 197.
  - [12] B. R. Parry, I. V. Surovtsev, M. T. Cabeen, C. S. O'Hern, E. R. Dufresne, and C. Jacobs-Wagner, *Cell* **156**, 183 (2014).
  - [13] M. Guo, A. J. Ehrlicher, M. H. Jensen, M. Renz, J. R. Moore, R. D. Goldman, J. Lippincott-Schwartz, F. C. Mackintosh, and D. A. Weitz, *Cell* **158**, 822 (2014).
  - [14] K. Yasuda, R. Okamoto, S. Komura, and A. S. Mikhailov, to be published in EPL.
  - [15] K. Yasuda, R. Okamoto, and S. Komura, to be published in *Phys. Rev. E*.
  - [16] J.-B. Manneville, P. Bassereau, D. Lévy, and J. Prost, *Phys. Rev. Lett.* **82**, 4356 (1999).
  - [17] J.-B. Manneville, P. Bassereau, S. Ramaswamy, and J. Prost, *Phys. Rev. E* **64**, 021908 (2001).
  - [18] S. Ramaswamy, J. Toner, and J. Prost, *Phys. Rev. Lett.* **84**, 3494 (2000).
  - [19] A. S. Mikhailov and R. Kapral, *Proc. Nat. Acad. Sci. USA* **112**, E3639 (2015).
  - [20] R. Kapral and A. S. Mikhailov, *Physica D* **318-319**, 100 (2016).
  - [21] Y. Koyano, H. Kitahata, and A. S. Mikhailov, *Phys. Rev. E* **94**, 022416 (2016).
  - [22] M.-J. Huang, A. S. Mikhailov, and H.-Y. Chen, *Eur. Phys. J. E* **35**, 119 (2012).
  - [23] M.-J. Huang, R. Kapral, A. S. Mikhailov, and H.-Y. Chen, *J. Chem. Phys.* **138**, 195101 (2013).
  - [24] M. Tanaka and E. Sackmann, *Nature* **437**, 656 (2005).
  - [25] S. Ramachandran, S. Komura, K. Seki, and G. Gompper, *Eur. Phys. J. E* **34**, 46 (2011).
  - [26] S. Ramachandran, S. Komura, K. Seki, and M. Imai, *Soft Matter* **7**, 1524 (2011).
  - [27] S. Komura, S. Ramachandran, K. Seki, and M. Imai, *Advances in Planar Lipid Bilayers and Liposomes* **16**, 129 (2012).
  - [28] K. Simons and E. Ikonen, *Science* **290**, 1721 (1997).
  - [29] S. Komura and D. Andelman, *Adv. Colloid Interface Sci.* **208**, 34 (2014).
  - [30] D. Lingwood and K. Simons, *Science* **327**, 46 (2010).
  - [31] H. Diamant, *J. Phys. Soc. Jpn.* **78**, 041002 (2009).
  - [32] N. Oppenheimer and H. Diamant, *Biophys. J.* **96**, 3041 (2009).
  - [33] N. Oppenheimer and H. Diamant, *Phys. Rev. E* **82**, 041912 (2010).
  - [34] E. P. Petrov and P. Schuille, *Biophys. J.* **94**, L41 (2008).
  - [35] E. P. Petrov and P. Schuille, *Soft Matter* **8**, 7552 (2012).
  - [36] S. Komura, K. Yasuda, and R. Okamoto, *J. Phys.: Con-*

dens. Matter **27**, 432001 (2015).

[37] A. W. C. Lau and T. C. Lubensky, Phys. Rev. E **80**, 011917 (2009).